Space Weather

RESEARCH ARTICLE
10.1029/2018SW001821

Evaluating the Skill of Forecasts of the Near-Earth Solar Wind Using a Space Weather Monitor at L5

S. R. Thomas[1,2], A. Fazakerley[2], R. T. Wicks[2,3], and L. Green[2]

[1]Jeremiah Horrocks Institute, University of Central Lancashire, Preston, UK, [2]Mullard Space Science Laboratory, University College London, Dorking, UK, [3]Institute for Risk and Disaster Reduction, University College London, London, UK

Key Points:
- We quantify the ability to forecast solar wind parameters from one spacecraft to another, 60° apart in heliographic longitude
- We find good agreement in most parameters between the forecasted data from the first spacecraft to the observed data from the second
- Skill scores show that a solar wind forecast from L5 would perform better than using persistence from one solar rotation before

Correspondence to:
S. R. Thomas,
sthomas17@uclan.ac.uk

Citation:
Thomas, S. R., Fazakerley, A., Wicks, R. T., & Green, L. (2018). Evaluating the skill of forecasts of the near-Earth solar wind using a space weather monitor at L5. *Space Weather*, *16*. https://doi.org/10.1029/2018SW001821

Received 3 FEB 2018
Accepted 5 JUN 2018
Accepted article online 19 JUN 2018

Abstract Forecasting space weather is an essential activity for increasing the resilience of modern technological infrastructure to hazards from the Sun. To provide an accurate forecast, space weather monitors positioned at L5 are proposed that carry in situ plasma detectors. Here we use data from the STEREO and ACE missions to investigate how well it is possible to predict the solar wind when there are two spacecraft located with the same longitudinal separation as from L5 to Earth. There are four intervals when this is the case: STEREO-to-STEREO both on the Earth's side and the far side of the Sun, STEREO-B to ACE and ACE to STEREO-A. We forecast the solar wind by mapping the observed solar wind at the first spacecraft to the second using a time delay calculated using the spacecraft's heliographic longitudinal separation and the difference in radial distance from the Sun, allowing for the solar wind speed. Using forecasting skill scores, we find that the predicted and observed solar wind data are, in general, in very good agreement with each of the four periods, including observed corotating interaction regions. However, there are some notable exceptions when corotating interaction regions have been missed by the forecast. The skill improves further for all time periods when removing coronal mass ejections, which cannot be predicted in this method. We suggest that an L5 monitor should be located at the same heliographic latitude as the Earth to optimize the forecasting ability of the monitor and to reduce the chance of missing important events.

Plain Language Summary A space weather monitor spacecraft has been proposed away from the Earth's viewing direction, which is likely to help improve the warning of solar events that could be heading towards Earth. In this study, we investigate whether such a spacecraft can improve our predictions of important physical values that are associated with the solar wind. To do this, we use times when two spacecraft have previously been in similar locations with respect to each other and map each value from one spacecraft to the other, making several important considerations relating to the spacecraft's motion and the movement of the plasma that they are embedded within. We have used "skill scores," which are used to assess weather forecasts to quantify how well our forecast performs. We find that a spacecraft at this location predicts almost all important values better than relying on a spacecraft at L1. This means that a detector of these parameters is essential for when the mission is commissioned.

1. Introduction

Space weather forecasting has been taken up by many global forecasting institutes, including the UK Met Office and NOAA in the United States. The main forms of solar activity that drive severe space weather and that are considered key to mitigating hazards at Earth are as follows: eruptions of plasma and magnetic field, known as coronal mass ejections (CMEs); compression regions caused by fast solar wind catching up to slower wind ahead of it, known as corotating interaction regions (CIRs); high-speed streams originating from coronal holes; and high-intensity bursts of radiation and energetic particles associated with solar flares and fast CMEs with strong interplanetary shocks (e.g., Klein & Dalla, 2017). CMEs and CIRs cause compressions in the solar wind and heliospheric magnetic field, which can influence the Earth's magnetosphere (Dungey, 1961) and cause hazards for humans and human technology in near-Earth space and at the surface (Hapgood, 2011).

CIRs and the irregular but more intense CMEs cause geomagnetic storms that can increase the energy and density of radiation belt electrons and protons, which in turn can degrade the performance of satellites

and may cause permanent damage to them. Geomagnetic storms also cause intense ionospheric currents that lead to geomagnetically induced currents in high-voltage or otherwise highly conducting infrastructure on the ground. The changing conditions in the solar wind thus constitute one of the main components of space weather and pose a risk to space-based and ground-based technological critical infrastructure. The financial cost of space weather to the world economy is still debated, but recent studies (e.g., Eastwood et al., 2017; Oughton et al., 2016) have estimated that a severe space weather event could cost up to 333.7 billion dollars.

In order to provide space weather forecasts with a longer lead time, several mission concepts have been proposed. Some of the mission concepts propose to utilize the L5 point, located 60° behind the Earth in its orbit, meaning that a spacecraft located at L5 will pass over the same region of the solar surface as the Earth about 4 to 5 days before the Earth. Any solar wind features determined by source region, for example, the large-scale solar wind stream structure, especially CIRs, will thus hopefully be observed at L5 4 or 5 days in advance of arriving at Earth. Suggested missions included the Earth-Affecting Solar Causes Observatory (Gopalswamy et al., 2012), Instant (Lavraud et al., 2014), and Carrington (Trichas et al., 2015). The benefits of such a mission are as follows: a side-on view to more accurately track Earth-directed CMEs and predict their arrival time, an early view of active regions on the Sun to deduce the probability of a CME being released towards Earth, the impact of a CIR on the probe at L5 before it rotates to Earth could give an early warning of intense CIRs arriving at Earth and magnetogram images, or magnetographs of the east limb of the Sun could help to improve magnetohydrodynamics models of the solar corona and solar wind (Auchere & Gopalswamy, 2014).

The STEREO spacecraft have often been used to give stereoscopic observations of CMEs to predict whether or not they will hit Earth (e.g., de Koning & Pizzo, 2011; Mishra & Srivastava, 2013; Tucker-Hood et al., 2015). However, STEREO also gives us an excellent opportunity to investigate how a monitor at L5 could be used to improve space weather forecasting. STEREO-A and STEREO-B were launched in 2006 and have drifted ahead/behind Earth within its orbit. In late 2009, STEREO-B crossed the L5 point 60° behind Earth in its orbit, providing an opportunity to compare data from the region of L5 to near-Earth space (Turner & Li, 2011). Turner and Li (2011) used cross-correlations of a number of heliospheric parameters between STEREO and ACE over a 1-year period during the solar minimum in 2008 to 2009. They showed that the solar wind speed is the most predictable from L5 with a time offset of 71 hr during this period. There were also positive correlations for solar wind density and magnetic field strength. Miyake et al. (2005) computed the correlation of L5 data with a nonsolar wind speed-corrected time lag and compared this to data from L1, one solar rotation previously. They found that the correlation from L5 was significantly improved compared to that from L1 27 days before.

A simulation of the solar wind at ACE was produced by Simunac et al. (2009) by extrapolating data from L5 and including the effect of the solar wind speed between the radius of STEREO-A and that of ACE (STEREO-A orbits with a smaller radius than ACE, which has a smaller orbital radius again than STEREO-B). They then compared their simulation with data from L1 and found a good correlation, mostly within the uncertainty on their simulation. However, they did not expand their study to include the whole of the range when STEREO-A and ACE were 60° apart, instead focussing on a shorter period including two CIRs. In this study we aim to build on the work of Simunac et al. (2009) by expanding the time period studied and to include all times when there have been two spacecraft 60° apart from one another in heliocentric orbit. Additionally, we use forecasting metrics, such as the skill score used in Owens et al. (2013) and adapted from meteorological forecasting (e.g., Roebber, 1998), to assess how well we can forecast the solar wind at L1 from observations at L5. Forecasting the solar wind conditions at L1 is key for improved space weather forecasts, because the impact of the solar wind conditions and eruptive events, such as CMEs, CIRs, and high-speed streams, drive space weather at Earth. Furthermore, CMEs themselves interact with the solar wind so that their evolution and propagation time are affected. CMEs cannot be predicted with this method because they are transient events with lifetimes shorter than 4 days in the inner heliosphere. CIRs can be predicted because the lifetime of a coronal hole can be several solar rotation periods. The most severe CIRs can cause space weather effects similar to CMEs (Denton et al., 2006).

2. Predicting the Solar Wind Using Spacecraft 60° Apart

For this study, we find times when two spacecraft out of the STEREO-A, STEREO-B, and ACE collection have a heliographic longitude separation of 60°. As the STEREO spacecraft move apart from one another and ACE with time, we select a 10° interval when the spacecraft are separated by heliographic longitudes of 55° – 65°

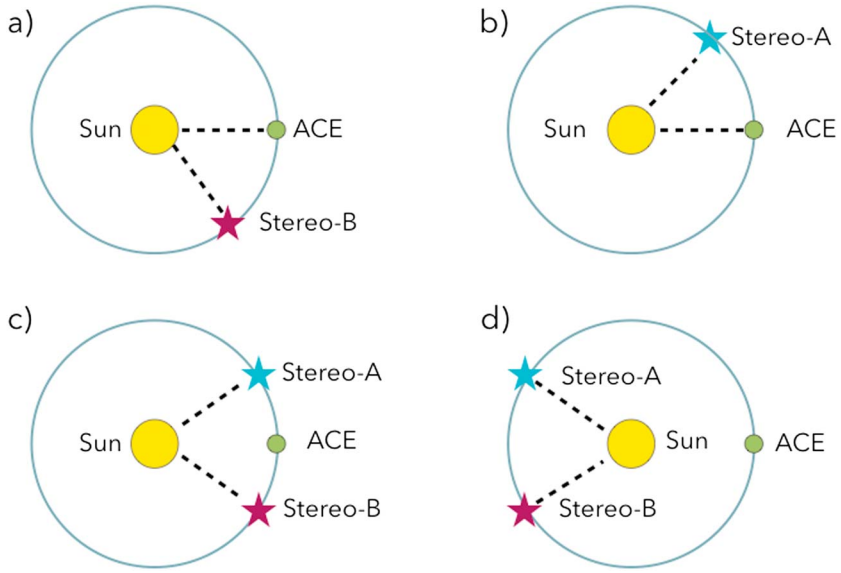

Figure 1. A schematic (in the ecliptic plane) of the spacecraft positions for the four time periods when there are two spacecraft approximately 60° apart, which can be used to approximate the L5–L1 configuration. In this diagram the Sun and solar wind rotate in an anticlockwise direction.

to simulate the L5 to L1 distances. Between 2006 and the present, there have been four periods when two spacecraft have been within this angular separation of one another. Each of these situations are shown in Figure 1 and are as follows: (a) STEREO-B to ACE, (b) ACE to STEREO-A, (c) STEREO-B to STEREO-A, and (d) STEREO-A to STEREO-B (the opposite side of the Sun to Earth). In each of these cases, we predict the solar wind at the second spacecraft (analogous to L1) from the data at the first (analogous to L5), in a similar manner to Simunac et al. (2009).

To map the observed solar wind parameters from one spacecraft to the other, we first account for the longitudinal separation of the two spacecraft and then add an additional displacement due to the difference in radial position. First, we consider the time delay between the spacecraft. For each spacecraft we simply apply a time difference to the data from the first spacecraft, which corresponds to the time taken for the source region on the Sun to rotate from facing the first spacecraft to the second. The solar rotation period at the equator is assumed to be 27 days. Thus, the time taken for solar wind from a particular source region on the Sun to be observed at L5 until solar wind from the same region is observed at L1 is, on average, around 4.5 days. We note that this time difference increases with time as the spacecraft separation in longitude increases.

Second, we account for the distance from the Sun by using the difference in radial distance divided by the solar wind speed. Combining the longitudinal separation (with time) and the radial separation terms results in equation (1), derived first by Simunac et al. (2009) but applied here to the heliographic longitude rather than Carrington longitude. Here $\phi_{\mathrm{mod}}(t)$ is the modelled longitude of the time-shifted data, $\phi_{\mathrm{obs}}(t)$ is the longitude of the spacecraft taking the role of the L5 monitor, Ω is the angular speed of rotation of the Sun, v_{sw} is the solar wind speed measured by the L5 monitor, R_{obs} is the radial distance from the Sun of the L1 monitor, and R_{mod} is the radial distance of the L5 monitor. ϵ is an error term included to account for the potential difference in latitude of the two spacecraft.

$$\Phi_{mod}(t) = \Phi_{obs}(t) - \frac{\Omega_{Sun}(R_{obs} - R_{mod})}{v_{sw}} + \epsilon \quad (1)$$

The derived change in heliographic longitude is then converted into the time taken for the solar wind to get from the leading spacecraft to the trailing using the angular solar rotation speed. The total time taken for solar wind from a given source to be observed at the first spacecraft and then the second is thus these converted times plus the difference in time due to the heliographic longitudinal separation of the two spacecraft calculated simply by multiplying the angular separation of the two spacecraft, which changes by time, by the solar rotation rate, Ω.

The calculations of the time delay from the first spacecraft to encounter the solar wind to the second are thus computed for all four scenarios outlined in Figure 1. These are then applied to the data from the first spacecraft to compare with the second. This way we expect to observe long-lasting solar wind features, such as CIRs, in both data sets simultaneously (when including the time-delay) but not more local and impulsive events such as CMEs as these frequently only cross one of the two spacecraft. There are, however, some key assumptions with mapping data between the spacecraft in this manner. The method assumes that both the evolution of the Sun and the solar wind do not change within the time taken from the solar wind source to rotate from being connected to one spacecraft to the other. This assumption is reasonable as most solar regions do not appear or disappear on timescales less than one solar rotation, although active regions, for example, do change shape more rapidly on these spatial and temporal scales (e.g., Scrijver & De Rosa, 2003). Second, the rate of change of solar activity is affected by the solar cycle and so our predictions are likely to be most accurate when the Sun's activity is not changing much with time (i.e., at solar minimum and not when the Sun is quickly increasing or decreasing with activity).

We apply the calculated time delays to several important solar wind parameters; the solar wind speed (|v|), plasma density (n_p), plasma temperature (T_p), magnetic field strength (|B|), and the north-south component of the magnetic field (B_z), each in hourly resolution. Skill scores are used to quantitatively assess the performance of our mapping technique. These are adapted from those used to deduce the performance of weather forecasts. We compare the prediction of solar wind conditions from 60° ahead with the conditions from one full solar rotation (360°) previous to the period.

We also compute the cross-helicity, σ_C, from the 5-min solar wind velocity and magnetic field components as a proxy for the locations of increased large amplitude Alfvénic fluctuations. The 5-min resolution is necessary to investigate the data for times of Alfvén wave activity (e.g., Mattheaus & Goldstein, 1982, Wicks et al., 2013), which fluctuates the solar wind velocity and magnetic field vectors substantially on this timescale. To compute the cross-helicity mathematically, the magnetic field values are first normalized into Alfvén speed units by equation (2), where μ is the permeability of the vacuum, n_i is the solar wind ion number density, and m_i is the ion mass.

$$B_A = \frac{B}{\sqrt{4\pi\mu n_i m_i}} \tag{2}$$

The cross-helicity, σ_C, can then be found from equation (3), where δv is the difference between consecutive solar wind velocities and δB_A is the difference between consecutive magnetic field values.

$$\sigma_C = \frac{2|\delta\vec{v}.\delta\vec{B}_A|}{\delta v^2 + \delta B_A^2} \tag{3}$$

σ_C is calculated and then normalized via equation (3) such that the maximum σ_C, and the remainder of the data is scaled accordingly (as was also implemented in Thomas et al., 2014). A 1-hr average of the modulus of σ_C is taken. This is so that we are able to still detect Alfvén waves, but the small-scale fluctuations are not so extreme for the purposes of this study (large fluctuations over a few minutes are unlikely to be forecastable over such large distances between the two spacecraft).

Alfvén waves are likely to be sustained in similar locations as the Sun rotates and are thus more predictable than B_z, and can influence the Earth's magnetosphere when they impact from the solar wind (Tsurutani et al., 2006). The cross-helicity also allows us to investigate the presence of large-amplitude Alfveń waves in the solar wind, which could act to scatter high-energy particles such as solar energetic particles and galactic cosmic rays (e.g., Lazarian, 2016).

3. Using Meteorological Skill Scores to Measure Predictability in Solar Wind

To quantify the performance of our solar wind forecasts, we use meteorological skill scores, as presented by Owens et al. (2013) who used the skill scores to assess the performance of their 27-day persistence solar wind forecasts. To calculate the skill of a forecast, the mean square error (MSE) of the forecast with respect to the observations must first be calculated using equation (4) (Roebber, 1998), where N is the number of samples

in the data, and X_{obs} and X_{mod} are the observed values of a heliospheric parameter at a given time in the observed and translated data series.

$$MSE = \frac{1}{N}\sum_{t=1}^{N}[X_{obs}(t) - X_{mod}(t)]^2 \quad (4)$$

We compute the MSE for all four spacecraft configurations and for each heliospheric parameter. The MSEs can then be used as an input to compute the skill scores in equation (5), where MSE_{mod} is the MSE calculated for each heliospheric parameter from equation (3) and MSE_{ref} is the MSE calculated for a reference forecast, in this case a persistence forecast, described below.

$$Skill = 100\left(1 - \frac{MSE_{mod}}{MSE_{ref}}\right) \quad (5)$$

The skill score works by having a reference forecast to compare the new forecast to and is thus a measure of how well the new forecast performs compared to this reference. For the purpose of generating a reference forecast, Owens et al. (2013) used randomly selected solar wind data, generated from a probability distribution of each heliospheric parameter that is typical of the solar wind. However, for our study it makes sense to compare our L5 forecast to the best purely observational solar wind forecasting method we can currently achieve operationally: a persistence forecast from L1 one solar rotation before, based upon the assumption that the solar wind does not change from one solar rotation to the next. The persistence forecast uses a time delay, which is simply calculated as one solar rotation, accounting for the fact that Earth has moved in its orbit during that time. The resulting skill scores have meaning as follows:

1. If $MSE_{mod} = MSE_{ref}$ then the skill score will be zero indicating the simulated forecast is equally well predicting the observations as the reference.
2. If $MSE_{mod} > MSE_{ref}$ then the skill score will be negative indicating that the simulated forecast is performing less well than the reference.
3. If $MSE_{mod} > MSE_{ref}$ then the skill score will be positive indicating that the simulated forecast is performing better than the reference.
4. If $MSE_{mod} >> MSE_{ref}$ then the skill score will tend towards $-\infty$ indicating a very poor forecast.
5. If $MSE_{mod} << MSE_{ref}$ then the skill score will tend towards 100 indicating a very strong forecast.
6. If $MSE_{mod} = 0$ then the simulated forecast is perfect and the skill score is 100.

From the skill scores deduced from equations (3) and (4) and by analyzing the outputs for each heliospheric parameter during each time period, we can deduce how our forecasting method from the STEREO data compares to using data from one solar rotation previously from L1 data.

4. Removal of CMEs From the Data

Previous studies either compared the forecasted data to the observations visually (Simunac et al., 2009), statistically (Turner & Li, 2011), or for a persistence forecast using skill scores for all available data (Owens et al., 2013). Here we remove CMEs from within the data set because this method of solar wind forecasting cannot forecast CMEs because they are transient features on a timescale shorter than a few days, rather than recurring or persistent structures. We instead forecast the ambient solar wind, fast solar wind streams, and CIRs. A large CME is likely to only impact one spacecraft or to impact both but without the time lag we calculate from the solar wind speed and impart on the data. CMEs are often associated with large solar wind compression, which can, for extreme examples, increase the local solar wind magnetic field strength from approximately 5 nT to more than 50 nT (e.g., Liou et al., 2014; Thomas et al., 2015). Therefore, CMEs will increase the MSE of our data substantially, having a very significant impact on the resulting skill scores.

To remove CMEs fairly, we use CME catalogues created from ACE (Liu et al., 2010; Richardson & Cane, 2010) and STEREO (Jian et al., 2013; Liu et al., 2010) in situ records. As each CME catalogue is compiled using different criteria for the identification of CMEs from the in situ data, the Liu et al. (2010) catalogues from STEREO and ACE/WIND are utilized, with comparisons taken with the Richardson and Cane (2010) and Jian et al. (2013) catalogues. We find CMEs for each spacecraft, for the time period in consideration and for the previous solar rotation, to ensure consistency between the simulated and reference forecasts. Furthermore, for each recorded CME we remove all data from the simulated and reference forecasts, as well as the observations between the onset and ending times of the CME observation at the spacecraft, to ensure that the data length, N, in equation (4) is constant for all calculations.

The change in the skill scores from removing the CMEs for most periods is likely to be small for the intervals displayed in Figure 1, as they are all between 2008 and 2010, when the Sun was in the deep minimum of Solar Cycle 24, and hence, there were very few CMEs (Lockwood et al., 2012). The in situ CME catalogues, listed above, reflect this with very few CMEs in any period, and the most of which showing very little enhancements in the solar wind parameters when observed in situ (with the exception of the intensity of the magnetic field strength observed during 10–13 December 2013). Thus, we expect only a minor variation in the skill scores for each time period with or without the CMEs, apart from the relatively short time period between November 2013 and January 2014.

For use in space weather forecasting using a potential future monitor at L5, the process of finding CMEs in the in situ data at L5 must be automated to allow for the swift removal of data from the skill score calculation procedure. This could be done by looking for "typical" changes in heliospheric parameters caused by CMEs (e.g., Webb & Howard, 2012, and references therein) or by tracking such a CME from heliospheric imagers from on-board other spacecraft (Savani et al., 2012).

5. Comparing Solar Wind Predictions to Observations

We now present a comparison between our forecasts from our theoretical L5 spacecraft and the observations seen at the second spacecraft, 60° behind in arrival of solar wind from a static source region on the Sun. In each time period, we compute forecasts for the hourly radial solar wind speed, $|v_x|$; plasma density, n_p; plasma temperature, T_p; magnetic field strength, $|B|$; and north-south component of the magnetic field, B_z. We also compute σ_C to investigate the predictability of large amplitude Alfveń waves from 60° ahead in the Sun's rotation. Finally, we display the heliographic latitude of each spacecraft to show times when both spacecraft are sampling solar wind from similar sources but at different times, or potentially from different sources due to the large latitudinal separation.

Figure 2 shows the first of the comparisons between the propagated and observed parameters, which is summarized by the orientation of the spacecraft shown in Figure 1c. These spacecraft were 55°–65° apart between 11 June and 5 August 2008, and so the data between these dates are displayed. Here we display a number of heliospheric parameters as measured by STEREO-A (black line) and as forecasted from STEREO-B (red line). The hourly maximum of the modulus of the cross-helicity, labelled σ_c, for both STEREO-A and STEREO-B is also given. This maximum is taken as to be able to compute skill scores in the same manner as other heliospheric parameters and is enhanced during times of significant Alfén wave activity. The integrated negative B_z, which is useful for examining whether it is possible to forecast timings of the solar wind most geoeffective magnetic field configurations, is next shown, and finally, the heliographic latitudes of STEREO-A and STEREO-B are shown, which are color coded in a similar manner as the heliospheric parameters, with STEREO-A in black and STEREO-B in red. The blue shaded regions show times when a CME was present in the CME catalogues, and hence, the data within these regions was removed for the final skill score calculations (shown in the next section).

The period analyzed by Simunac et al. (2009) is included within the time period of Figure 2 from day of year 183 to 213. During this time period, our predictions from STEREO-B to STEREO-A are in good agreement with their results as our forecast matches well to the observations throughout the period and is similar to the Simunac et al. (2009) predictions. This time period included the CIR beginning on day of year 195, which included a jump in speed of over 100 km/s and density and magnetic field enhancements that are indicative of a shock. We successfully predict the onset time from a spacecraft 60° ahead with respect to the Sun's rotation using our computed time lags to within 1 hr in the solar wind and magnetic field strength here. The timing of our forecasted CIR is also in good agreement with the forecast of Simunac et al. (2009). Our forecast, similar to the previous study, also appears to perform reasonably for the CIR beginning on day of year 205, which is associated with a weaker compression, although it does predict its arrival in the solar wind 2–3 hr early and the predicted velocity is higher than the measured velocity.

Prior to the time period analyzed by Simunac et al. (2009), the L5 prediction performs a little more inconsistently. The first CIR in the period is predicted very well with an onset on day of year 168. The intensity of the peak in each heliospheric parameter is well identified, and the prediction would have accurately described the observed event. However, the following CIR, with onset day of year 178, is far less well predicted from the preceding spacecraft. The CIR arrives 2 days earlier at STEREO-A than expected from STEREO-B

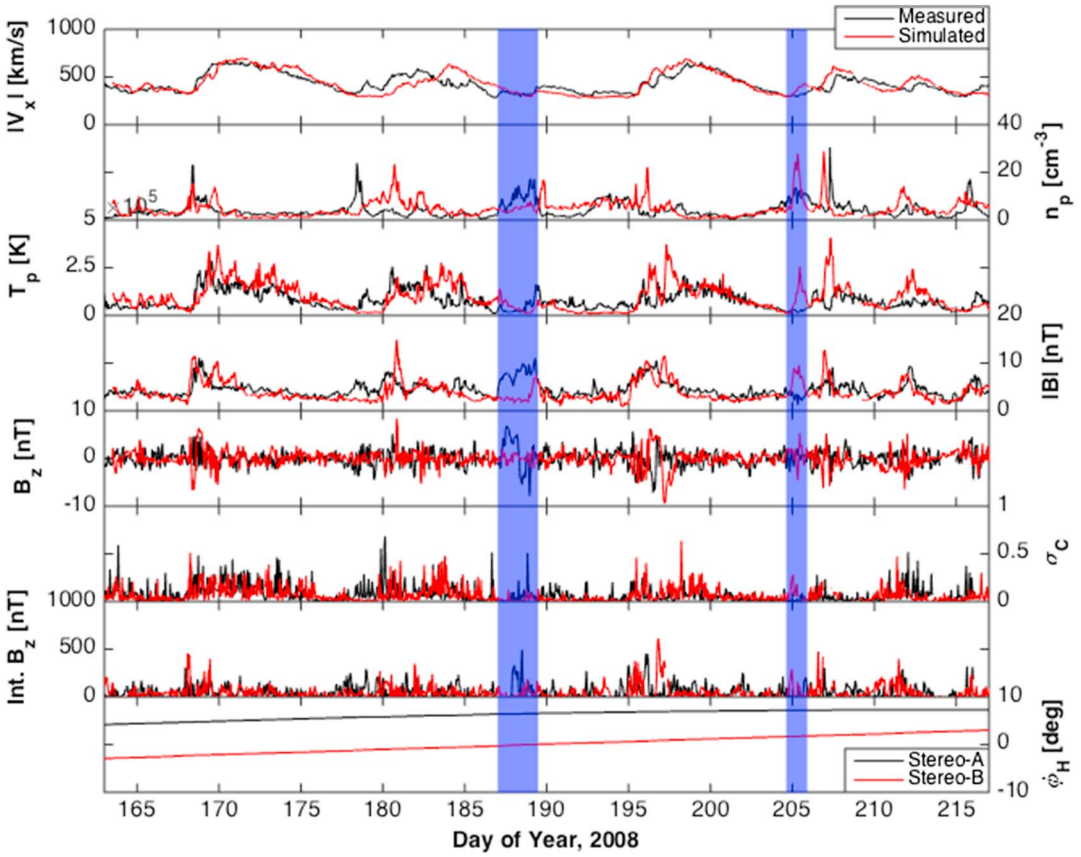

Figure 2. Time series from 11 June to 5 August 2008 (spacecraft orientation (c) from Figure 1) of, from top, radial solar wind speed, $|V_x|$; plasma density, n_p; plasma temperature, T_p; heliospheric magnetic field strength, $|B|$; north-south component of the magnetic field, B_z; cross-helicities for both spacecraft, σ_c; integrated negative B_z; and the heliographic latitudes, ϕ_H, of both spacecraft for STEREO-A (measured; black) and STEREO-B (predicted; red) with a time delay added based on the angular separation and solar wind speed. The shaded regions are times of coronal mass ejections.

as can be observed for each heliospheric parameter. Furthermore, the intensity of the peak is not well predicted from STEREO-B; the solar wind speed is 50 km/s faster from STEREO-B and the magnetic field magnitude was 7 nT greater.

This issue with the prediction of this CIR is not due to a CME but could instead be due to the large separation in the spacecraft latitudes throughout this period (approximately 8°). If a coronal hole boundary has a different longitude at different latitudes, then there will be an associate change in timing of CIR arrival as the spacecraft foot point will enter fast wind at different times. Indeed, Gosling et al. (1993) found that CIRs can have significant variation with latitude and so it is likely that the CIR simply had a different structure between these latitudes. Asymmetry of solar activity between the two hemispheres has previously been noted (e.g., Zou et al., 2014), which could play a role in the differing observations between the two spacecraft when the two spacecrafts are located on opposing sides of the heliospheric current sheet.

To explain why this event has not been well forecasted from ACE, we examine the source of the CIR at the Sun, (i.e., the boundary between a source of slow solar wind and a coronal hole). For this purpose, we use STEREO EUV 195Å data for the dates when the coronal hole was facing both STEREO-A and then STEREO-B approximately 4 days later. These images are shown in Figure 3. The STEREO-B data (right) indicates that there is a coronal hole that extends from southeast to northwest at this time, which is consistent with the timing differences between the two spacecraft. It is also clear from the images (4 days apart) that the coronal hole changes shape and weakens in the northern hemisphere, over the interval between measurements. The orientation of the coronal hole means that, with the spacecraft approximately 10° apart in heliographic latitude, one would expect the timings to be different for the associate CIR reaching the spacecraft. Furthermore, if the coronal hole is evolving in space, this could introduce further changes to the CIR and its timing

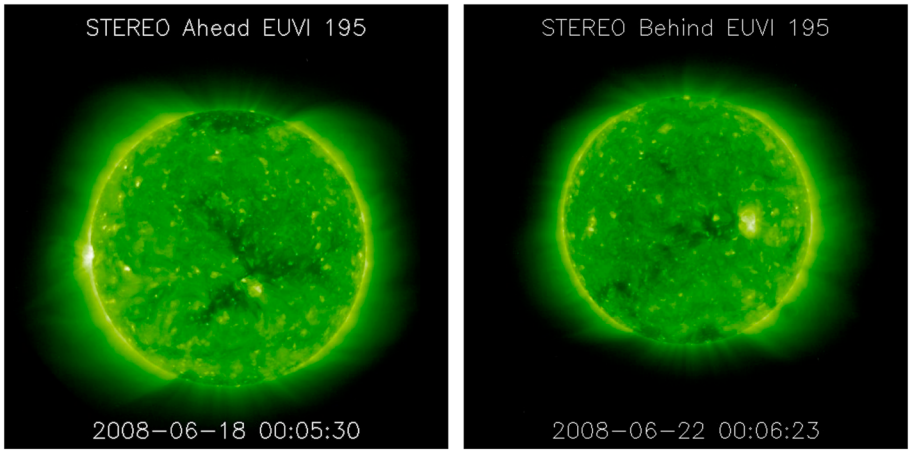

Figure 3. STEREO EUV 195 Angstrom images of the Sun from STEREO-A and STEREO-B on 18 and 22 June 2018, respectively, which shows the progression of a large equatorial coronal hole with time.

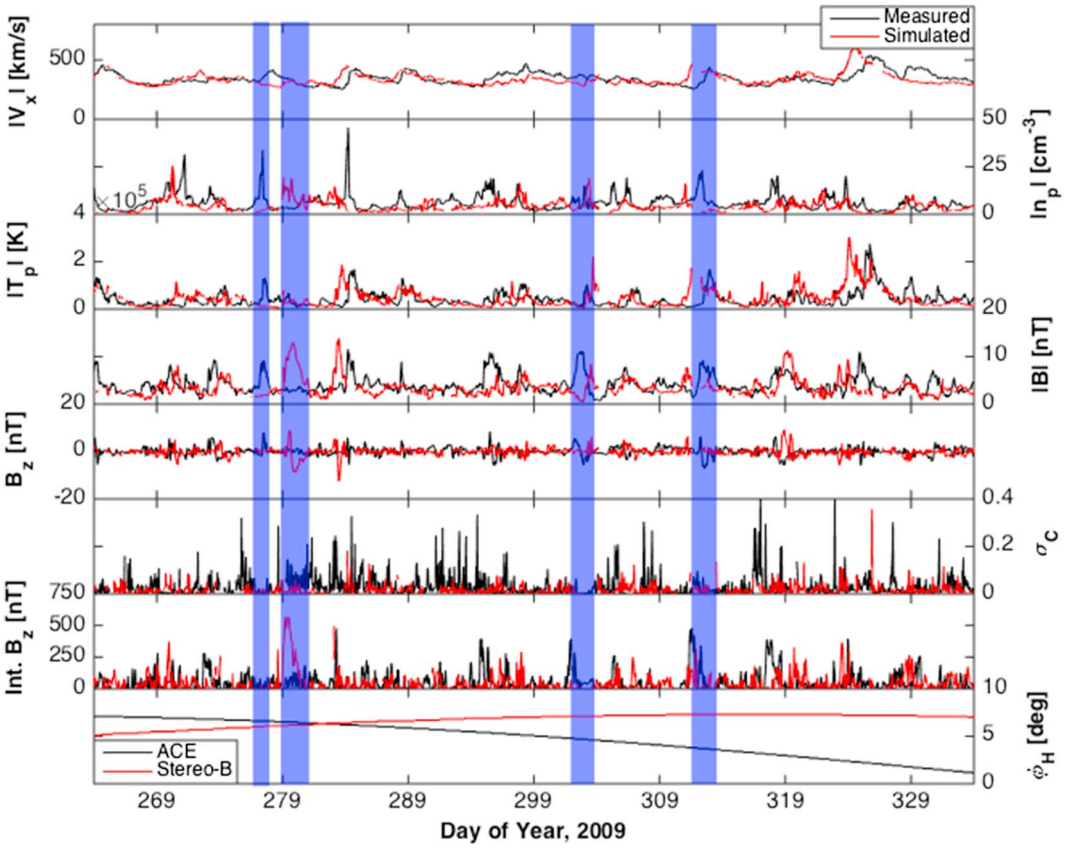

Figure 4. Time series from 22 September to 30 November 2009 (spacecraft orientation (a) from Figure 1) of, from top, radial solar wind speed, $|V_x|$; plasma density, n_p; plasma temperature, T_p; heliospheric magnetic field strength, $|B|$; north-south component of the magnetic field, B_z; cross-helicities for both spacecraft, σ_c; integrated negative, B_z; and the heliographic latitudes, ϕ_{hel}, of both spacecraft for ACE (measured; black) and STEREO-B (predicted; red) with a time delay added based on the angular separation and solar wind speed. The shaded regions are times of coronal mass ejections.

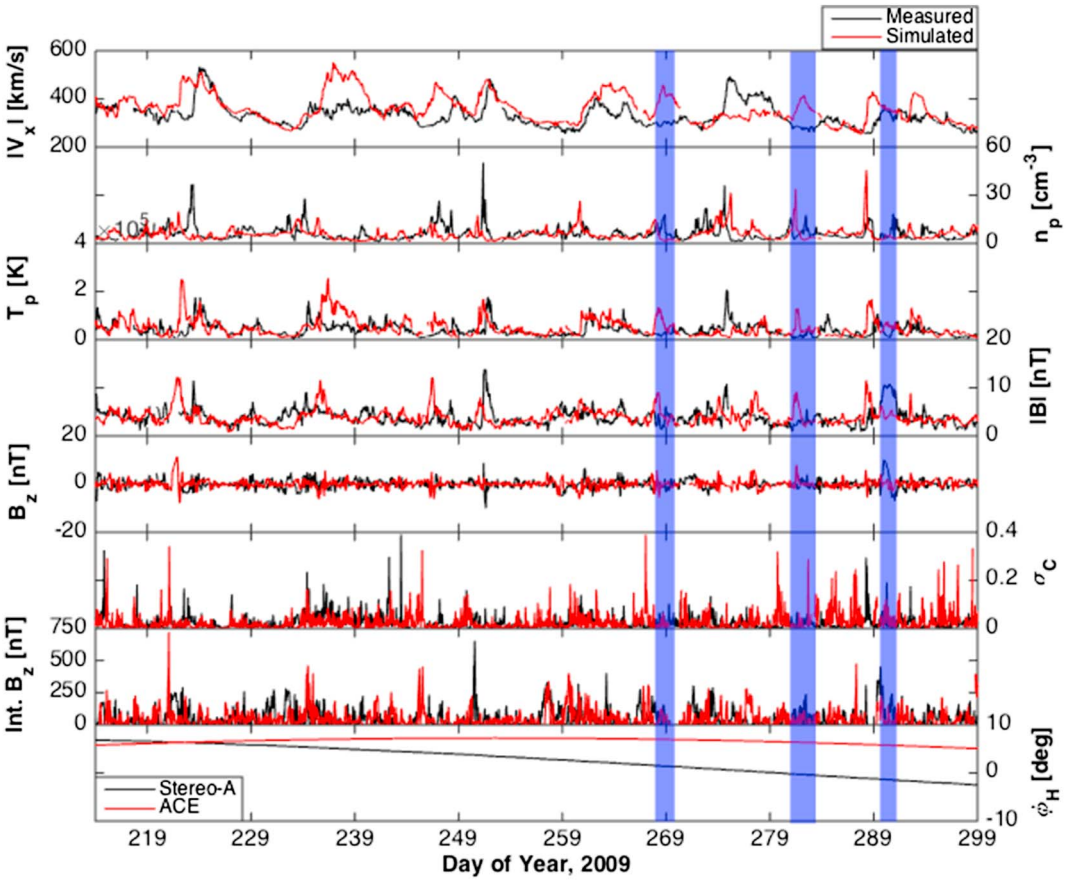

Figure 5. Time series from 2 August to 26 October 2009 (spacecraft orientation (b) from Figure 1) of, from top, radial solar wind speed, $|V_x|$; plasma density, n_p; plasma temperature, T_p; heliospheric magnetic field strength, $|B|$; north-south component of the magnetic field, B_z; cross-helicities for both spacecraft, σ_c; integrated negative, B_z; and the heliographic latitudes, ϕ_{hel}, of both spacecraft for STEREO-B (measured; black) and ACE (predicted; red) with a time delay added based on the angular separation and solar wind speed. The shaded regions are times of coronal mass ejections.

at the two spacecraft. It should be noted, however, that coronal hole synoptic maps, accessible from the NOAA website and created from Earth-perspective data, show a coronal hole with a only small extent.

Figure 4 shows the same as Figure 2 but for the scenario when STEREO-B and ACE were 60° apart during late 2009 (see Figure 1a), a time period not studied by previous L5-focussed studies. Here the solar wind forecast is mapping from STEREO-B to ACE and is compared to observations from ACE. During this period, there are four CMEs that are highlighted by the blue shaded regions, although all of which are fairly small events (Liu et al., 2010). There are also several CIRs both observed by ACE (black line) and forecasted from STEREO-B (red line). At the start of the time period, the timings and intensities of the CIRs are well predicted, especially in the solar wind speed. The CIR on day of year 263 is very well matched between the forecast and the observations. However, the CIR on day of year 283 is forecasted to arrive a few hours earlier than it is observed, although the intensity in most heliospheric parameters are well matched. During this time period, ACE and STEREO-B were located at very similar heliographic latitudes, shown by the bottom panel. Later in the time period, when the spacecraft are far more separated in heliographic latitude, the forecasted solar wind at STEREO-B is not so well matched to the observations.

Figures 5 and 6 show the same analysis as previous figures but compare the forecast data from ACE to observations from STEREO-A between 18 July 2009 and 3 February 2010 (see Figure 1b schematic). As the two spacecraft were in the range of 55°–65° from each other for approximately 7 months, we split the data between two figures. Figure 5, similarly to Figure 4 shows that, in all parameters, the forecast performs much better during the start of the period when the two spacecrafts were at similar heliographic latitudes than later in the period due to both spacecraft observing solar wind from the same source on the Sun. Indeed, the CIRs of days of year 252 and 261 are both very well predicted in timing and intensity from ACE.

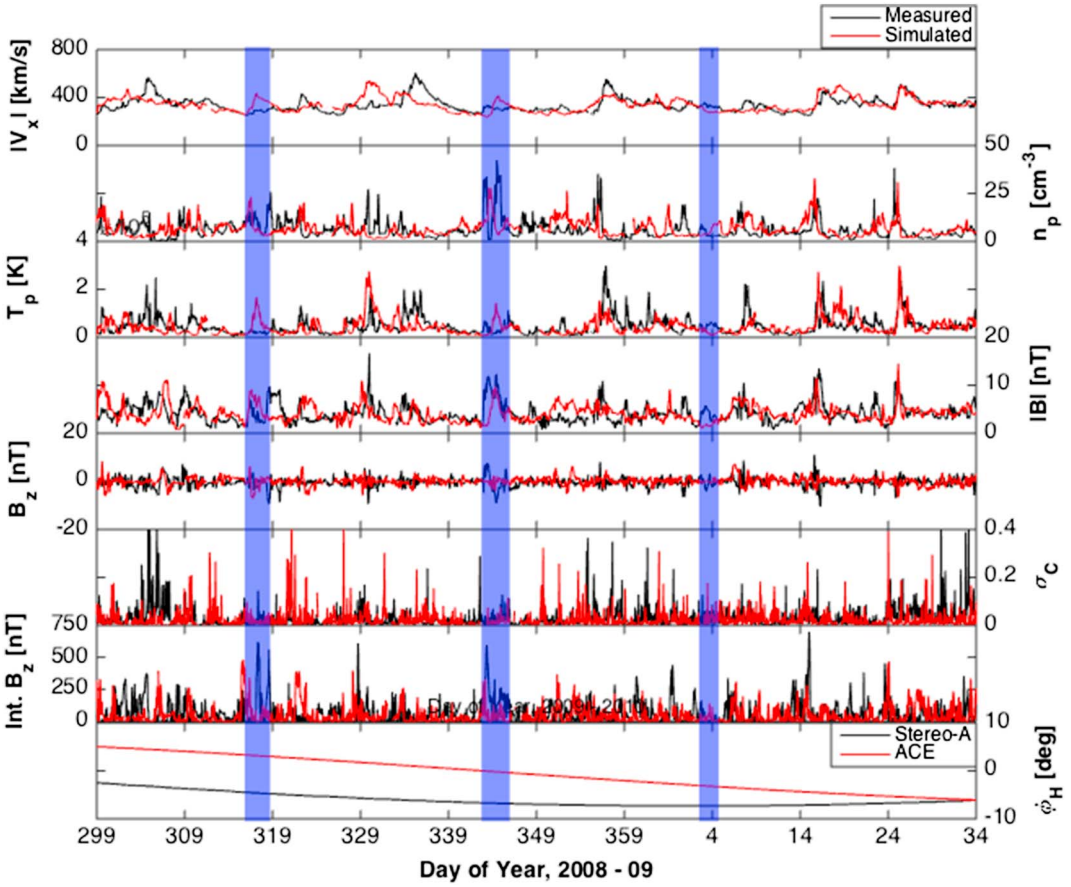

Figure 6. Time series from 26 October 2009 to 3 February 2010 (spacecraft orientation (b) from Figure 1) of, from top, radial solar wind speed, $|V_x|$; plasma density, n_p; plasma temperature, T_p; heliospheric magnetic field strength, $|B|$; north-south component of the magnetic field, B_z; cross-helicities, σ_c; integrated negative, B_z; and the heliographic latitudes, ϕ_{hel}, of both spacecraft for STEREO-A (measured; black) and ACE (predicted; red) with a time delay added based on the angular separation and solar wind speed. The shaded regions are times of coronal mass ejections.

There are, however, a few issues with the forecast from ACE. Shown on Figure 5, the CIR on day of year 235 gave higher values for the solar wind speed, plasma temperature, and magnetic field strength at ACE than at STEREO-A. For example, the solar wind speed from ACE was 150 km/s faster than observed at STEREO-A. During this period, the CIR decreased in intensity due to the evolution of the coronal hole causing the fast solar wind that has caused the CIR. At this time, Solar and Heliospheric Observatory EUV observations show small coronal holes in both hemispheres, suggesting that the spacecraft may be sampling compression regions from different CIRs.

The remainder of the time period when ACE and STEREO-A were 55° – 65° apart is shown in Figure 6. The CIR beginning on day of year 327 at STEREO-A is poorly predicted for the solar wind speed from ACE but is predicted much better in the other heliospheric parameters. The solar wind speed shows an increase from ACE, which coincides with the increase at STEREO-A and in each of the other solar wind parameters, but increases to approximately 550 km/s 5 days earlier than similar speeds are observed at STEREO-A. It is likely that ACE, during this event, observed two consecutive CIRs within 2 – 3 days of each other, associated with two coronal holes observed by Solar and Heliospheric Observatory and shown in Figure 6 by the twin peaks in magnetic field strength and plasma temperature, whereas STEREO-A only saw one CIR, from the single coronal hole in the southern hemisphere at the time. The predictions in the majority of the heliospheric parameters appear very strong for the remainder of the period as the spacecraft converge at a similar heliographic latitude.

Figure 7 shows the time period not previously considered for solar wind L5 studies, when STEREO-A and STEREO-B were 60° apart the other side of the Sun, between November 2013 and January 2014 (see Figure 1d schematic). During this time, the spacecraft were at a reasonably constant heliographic latitude separation of 6° – 7°. There are two CMEs removed from the data using the CME catalogues. The first, on day of year 340, is a particularly intense CME in all heliospheric parameters at STEREO-A and hence could give a huge error in

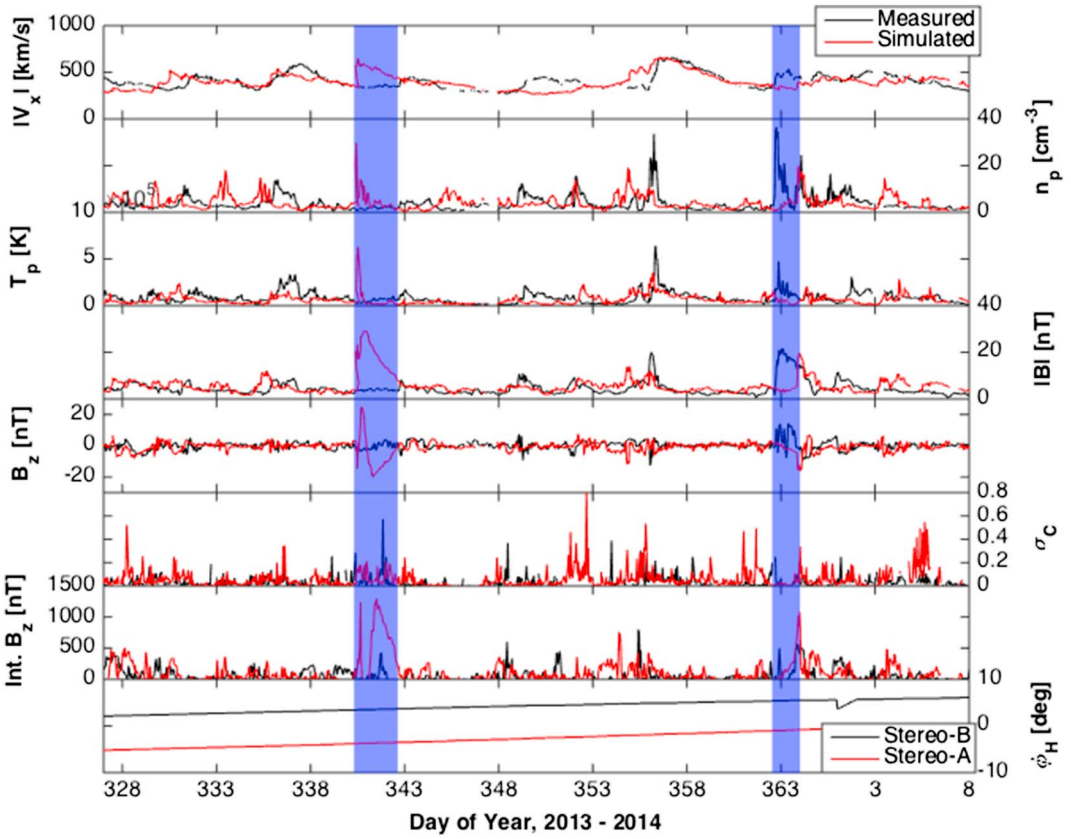

Figure 7. Time series from 23 November 2013 to 8 January 2014 (spacecraft orientation (d) from Figure 1) of, from top, radial solar wind speed, $|V_x|$; plasma density, n_p; plasma temperature, T_p; heliospheric magnetic field strength, $|B|$; north-south component of the magnetic field, B_z; cross-helicities, σ_c; integrated negative, B_z; and the heliographic latitudes, ϕ_{hel}, of both spacecraft for STEREO-B (measured; black) and STEREO-A (predicted; red) with a time delay added based on the angular separation and solar wind speed. The shaded regions are times of coronal mass ejections.

the MSE of the forecast leading to degradation in the skill score. There are also several CIRs during this time period, most notably the steepest and most intense CIR on day of year 355. The solar wind compression is observed earlier at STEREO-A (with the time delay included) than at STEREO-B. This early increase is also colocated with significant spikes in the plasma density and magnetic field, which could indicate the presence of a shock ahead of the main structure of the CIR (e.g., Gosling & Pizzo, 1999).

Although, generally the cross-helicity and integrated negative B_z are enhanced at the same times for the forecasted and observed data at the second spacecraft in each of Figures 2–7, small-scale structures in the data, such as spikes and short fluctuations in sign, are not well forecasted. With such quickly varying parameters, it is difficult to correctly forecast these short fluctuations without significant time averaging. The forecasts, for example, in Figure 2, do show promise in forecasting the timing and amplitude of Alfvén waves and B_z from one spacecraft to the next; such observations will now be quantified via the use of skill scores for each heliospheric parameter and each time period.

6. Analysis of Forecasting Skill

To quantify the ability of the forecasts from L5 to L1, we compute skill scores using equations (4) and (5) (Owens et al., 2013) for each of the heliospheric parameters shown on Figures 2–7. The skill scores are deduced without the inclusion of CMEs that are indicated by shaded regions in the figures and provide a comparison to a persistence forecast using data from the same spacecraft 27 days before, as the best solar wind forecasting using purely in situ measurements. Previously, this comparison has only been made by correlating solar wind parameters (Miyake et al., 2005) but no estimates have been made of forecasting skill.

In Table 1, we present the skill scores of each parameter during each spacecraft combination with the CMEs removed from the data. We remove these as CMEs cannot be forecasted using this method as they will either

Table 1
Skill Scores for Key Heliospheric Parameters Calculated for Each of the Spacecraft Configurations Displayed in Figure 1

Parameter	St-B to St-A	St-B to ACE	ACE to St-A	St-A to St-B	Total
$\|V_x\|$	−6.59	+34.07	+39.53	+55.11	+34.07
n_p	+21.57	+21.08	+18.06	−0.90	+12.13
T_p	−19.88	+18.65	+17.15	+37.02	+18.65
$\|B\|$	+10.84	+11.07	+19.68	+23.74	+17.46
B_z	+1.80	+2.39	+8.71	+1.98	+3.76
σ_C	+50.61	+43.20	−17.15	+4.12	+35.89
$IntB_z$	+1.27	−7.20	+4.13	−25.96	−10.56

Note. Coronal mass ejections have been removed from the data before the skill scores are calculated. The total is for all spacecraft configurations combined.

interact with only one of the spacecraft or interact with both at a similar time. We first concentrate on the top five rows. The first thing to note from Table 1 is that the majority of skill scores are positive indicating that the forecasts from 60° ahead in orbit are stronger than the persistence forecast from one solar rotation previously. Although this is expected, it is worth noting that a number of the skill scores are strongly in the positive (e.g., STEREO-B to STEREO-A solar wind speed has a skill score of +55.11) indicating that our forecast is considerably better than persistence. Note that the maximum skill score obtainable is +100. Additionally, for each parameter we calculate the skill scores for all of the time periods combined. These are displayed in the right-hand column of Table 1. For each of the top five heliospheric parameters, we find an increase in forecasting skill using an L5 monitor. This is particularly notable for the solar wind speed.

Second, some heliospheric parameters are better forecasted than others; the heliospheric magnetic field strength is positive, and in double figures, for all of the studied time periods and the solar wind speed, plasma temperature, plasma density, and cross-helicity are also consistently positive for three of the four periods. However, B_z is forecast poorly from the 60° separation, with most values near to zero, indicating no improvement from the persistence forecast. B_z has been found to be very difficult to predict in the solar wind for one solar rotation ahead (Turner & Li, 2011) especially at solar minimum (Owens et al., 2013). It is also known to change on short timescales in the solar wind without the presence of CMEs (Zhang et al., 2014) and so such a result may be expected.

Skill scores for the cross-helicity and the integrated B_z are also calculated. The cross-helicity is a good indicator of the presence of Alfvén waves and the integrated B_z gives an indication of how geoeffective the solar wind could be at any time. The cross-helicity is well predicted overall, with a skill score, for all the periods combined, of +35.89. It is very well predicted between STEREO-B and ACE (+43.20) and between STEREO-B and STEREO-A (+50.61), but poorly predicted between STEREO-A and STEREO-B (−17.15). From examining time series of the persistence and forecasts for the periods with the weaker skill (not shown), it appears that there are strong fluctuations observed from the first spacecraft, showing the presence of Alfvén waves, that are out of time with those observed at STEREO-B and hence are increasing the error. There is also a large fluctuation in the forecasted data from STEREO-A on day of year 351, which coincides with a data gap in the solar wind speed data from STEREO-B, which could account for an increased MSE for the forecast. On averaging the cross-helicity to a longer time series, it is likely that skill scores would improve but small wave trains will be lost in the averaging process. The integrated B_z, however, is much more poorly predicted with a total skill of −10.56. This further eludes to the idea that B_z is very difficult to predict.

We note that the skill scores are very different for each of the three spacecraft orientations studied. This difference arises due differences in the time the data were taken and the location of the spacecraft. The first three columns in Table 1 solar minimum conditions during 2008 and 2009, whereas the STEREO-A to STEREO-B case was in 2013 and 2014, during the weak solar maximum. Furthermore, the ACE to STEREO examples were approximately a year after the STEREO-B to STEREO-A example and so are sampling different solar wind conditions. Differences between STEREO-B and ACE and ACE and STEREO-A are due to the fact that they do not cover exactly the same time period due to their orbital motion with respect to Earth, and due to changes in the solar wind as it rotated between STEREO-A and STEREO-B. The time period most poorly forecasted from L5 was 2008 in most heliospheric parameters. This was mostly influenced by the poorly predicted CIR on day of year 178, addressed above, which was better predicted using the persistence forecast. Skill during each of the periods was also influenced by the solar wind conditions sampled. For example,

the negative skill for the plasma density in the STEREO-A to STEREO-B case was cause by the timing of a spike in the density being narrowly out from the forecast and thus contributing to the MSE twice.

A second cause for the differences between the time periods shown in Table 1 is that the plasma instruments on STEREO and ACE may become less well calibrated in time (Kohutova et al., 2016). If the sensitivity of different anodes within the instrument changes with time, and this is not corrected for by some kind of onboard calibration, one can very quickly observe serious errors the direction of the velocity vector. That may cause errors in cross-helicity (via the δV term in equation (3) when comparing measurements from two different spacecraft. From Table 1, we see that the skill of forecasting of cross-helicity is much greater in 2008 (+50.61) than in late 2009 (−17.15) or 2013 (+4.12). The forecasting skill also seems to decrease with time for the plasma density. One would not expect the same issue with magnetometers, which would explain why the same trend is not seen in the skill scores of the magnetic field. Thus, one would expect the 2008 period to be the most reliable time period for the cross-helicity skill score calculations, which suggests that large-amplitude Alfvén waves have predictability, which would be improved from an L5 monitor.

The overwhelmingly positive skill scores overall indicate that, during the four periods when we have two spacecraft separated by 55°–65°, an improved solar wind forecast is possible from L5 compared to using a persistence forecast (the best we can currently do observationally). The positive skill scores interestingly also include the cross-helicity, which is an indicator of Alfvén waves. These results could be combined with the improved forecasting of CMEs from L5 gained from having an additional vantage point in the heliosphere (Lugaz et al., 2010) to allow for consistently more accurate space weather monitoring.

7. Conclusions

We have investigated the skill of solar wind forecasting using spacecraft separated by 60° in heliospheric longitude to understand if a monitor at L5 could be used to predict the solar wind at Earth. To do this, we found four separate time periods when there have been two spacecraft 60° apart (in a similar arrangement to a monitor at L5 and Earth) using STEREO and ACE data. The data from the leading spacecraft was then mapped onto that of the trailing spacecraft, in the same manner as would be applied from L5 to Earth, allowing for the spacecraft separation, their different distances from the Sun, and the solar wind speed. The method uses two simple assumptions: (a) that the outflow from the source regions do not change on a 5-day timescale and (b) that the spacecrafts "see" outflow from the same source region. We often get good agreement that suggests that these are often reasonable assumptions. We thus compared time series and skill scores to assess the quality of our "L5" forecasts and concluded the following:

1. Forecasts produced by mapping data from the first spacecraft to encounter solar wind from a particular source to the next display mostly positive skill scores for all parameters with respect to a 27-day persistence forecast. The solar wind speed is particularly well matched. An average skill score of 50 for $|V|$ is found, implying that a useful forecast of $|V|$ can be made. On average, however, B_z has a skill score of approximately 0 and so no improvement in forecast can be made from L5 for this parameter.
2. Most CIRs over the four time periods are well predicted in intensity and timing in solar wind speed, plasma density, temperature, heliospheric magnetic field strength, and cross-helicity. Due to the enhancements in the heliospheric parameters when CIRs cross the spacecraft, if they are mistimed in the forecast, then CIRs could greatly increase the MSE of the forecast, and hence, the skill scores would be degraded. Given that we have predominantly positive skill scores from our forecast, it is clear that the CIRs are better predicted from L5 than using a persistence forecast.
3. There are, however, some events less well predicted by the forecast. For example, the CIR observed at STEREO-A on day of year 178 (27 June 2008) was very poorly predicted in most solar wind parameters (see Figure 2). This was due to the large latitudinal separation of the two spacecraft. Such a large difference in separation means that any unusually shaped coronal hole in latitude could result in the fast solar wind rotating into the spacecraft's path at different times. Furthermore, source regions on the Sun could evolve in time 4–5 days between the spacecraft encountering solar wind streams.
4. Cross-helicity, and thus large-amplitude Alfvén waves, is well forecasted from L5, particularly for the earliest time periods. This is likely due to the accuracy of the plasma instrument decreasing with time, as suggested by previous work. Any operational space weather mission plasma instruments thus would need to be designed in order to maintain the accuracy of the plasma measurements including the velocity vector as well as speed.

5. We suggest that an L5 monitor should be located at the same heliographic latitude as Earth, if possible, to optimize the forecasting ability of the monitor and to reduce the chance of missing important events. This is because the accuracy of the forecasts from L5 is degraded when the spacecraft are highly separated in latitude.

In general, our results show that an L5 monitor would improve the forecasting skill of the solar wind and CIRs compared to using data from one solar rotation previously. This information will combine with improvements in the predictability of CMEs from having an extra heliospheric vantage point (Lugaz et al., 2010) to improve space weather forecasting.

Acknowledgments
We acknowledge the use of the publicly available data from NASA's ACE and STEREO missions in this paper for which we are grateful for. The images in Figure 3 were sourced from the NASA STEREO mission image online archive. The work of S. R. T. is funded by the U.K. Space Agency International Partnership Space Programme (collaboration agreement L2796). A. N. F. is funded by UK STFC grant ST/H00260X/1. L. M. G. thanks the Royal Society for funding through the University Research Fellowship scheme.

References

Auchere, F., & Gopalswamy, N. (2014). Future L5 missions for solar physics and space weather. *40th COSPAR Scientific Assembly*, *D2.3*, 12–14.

de Koning, C. A., & Pizzo, V. J. (2011). Polarimetric localization: A new tool for calculating the CME speed and direction of propagation in near-real time. *Space Weather*, *9*, S03001. https://doi.org/10.1029/2010SW000595

Denton, M. H., Borovsky, J. E., Skoug, R. M., Thomsen, M. F., Lavraud, B., Henderson, M. G., et al. (2006). Geomagnetic storms driven by ICME- and CIR-dominated solar wind. *Journal of Geophysical Research*, *111*, A07S07. https://doi.org/10.1029/2005JA011436

Dungey, J. W. (1961). Interplanetary magnetic field and the auroral zones. *Physical Review Letters*, *6*, 47–48.

Eastwood, J. P., Biffis, E., Hapgood, M. A., Green, L., Bisi, M. M., Bentley, R. D., et al. (2017). The economic impact of space weather: Where do we stand? *Risk Analysis*, *37*, 206–218.

Gopalswamy, N., Davila, J. M., St Cyr, O. C., Sittler, E., Auchere, F., Duvall, T. L., et al. (2012). Earth-Affecting Solar Causes Observatory (EASCO): A potential international living with a star mission from Sun-Earth L5. *Journal of Atmospheric and Solar-Terrestrial Physics*, *73*, 658–663.

Gosling, J. T., Bame, S. J., McComas, D. J., Phillips, J., Pizzo, V. J., Goldstein, B. E., & Neugebauer, M. (1993). Latitudinal variation of solar wind corotating stream interaction regions: Ulysses. *Geophysical Research Letters*, *20*(24), 2789–2792.

Gosling, J. T., & Pizzo, V. J. (1999). Formation and evolution of corotating interaction regions and their three dimensional structure. *Space Science Reviews*, *89*, 21–52.

Hapgood, M. (2011). Towards a scientific understanding of the risk from extreme space weather. *Advances in Space Research*, *47*, 2059–2072.

Jian, L. K., Russell, C. T., Luhmann, J. G., Galvin, A. B., & Simunac, K. D. C. (2013). Solar wind observations at STEREO: 2007 - 2011. In *Proceedings of the Thirteenth International Solar Wind Conference. AIP Conference Proceedings* (pp. 191–194).

Klein, K.-L., & Dalla, S. (2017). Acceleration and propagation of solar energetic particles. *Space Science Reviews*, *212*, 1107–1136.

Kohutova, P., Bocquet, F.-X., Henley, E. M., & Owens, M. J. (2016). Improving solar wind persistence forecasts: Removing transient space weather events, and using observations away from the Sun-Earth line. *Space Weather*, *14*, 802–818. https://doi.org/10.1002/2016SW001447

Lavraud, B., Liu, Y. D., Harrison, R. A., Liu, W., Auchere, F., Gan, W., et al. (2014). Instant: An innovative L5 small mission concept for coordinated science with Solar Orbiter and Solar Probe Plus. American Geophysical Union, Fall Meeting 2014, abstract SH21B-4109.

Lazarian, A. (2016). Damping of Alfvén waves by turbulence and its consequences: From cosmic-ray streaming to launching winds. *The Astrophysical Journal*, *833*, 131.

Liou, K., Wu, C. C., Dryer, M., Wu, S. T., Rich, N., Plunkett, S., et al. (2014). Global simulation of extremely fast coronal mass ejection on 23 July 2012. *Journal of Atmospheric and Solar-Terrestrial Physics*, *121*, 32–41.

Liu, Y., Thernisien, A., Luhmann, J. G., Vourlidas, A., Davies, J. A., Lin, R. P., & Bale, S. D. (2010). Reconstructing coronal mass ejections with coordinated imaging and in situ observations: Global structure, kinematics, and implications for space weather forecasting. *The Astrophysical Journal*, *722*, 1762–1777.

Lockwood, M., Owens, M., Barnard, L., Davies, C., & Thomas, S. R. (2012). What is the Sun up to? *Astronomy & Geophysics*, *53*, 3.09–3.15.

Lugaz, N., Hernandez-Charpak, J. N., Roussev, I. I., Davis, C. J., Vourlidas, A., & Davies, J. A. (2010). Determining the azimuthal properties of coronal mass ejections from multi-spacecraft remote-sensing observations with STEREO SECCHI. *The Astrophysical Journal*, *715*, 493–499.

Mattheaus, & Goldstein, M. L. (1982). Measurement of the rugged invariants of magnetohydrodynamic turbulence in the solar wind. *Journal of Geophysical Research*, *87*(A8), 6011–6028. https://doi.org/10.1029/JA087iA08p06011

Mishra, W., & Srivastava, N. (2013). Estimating the arrival time of Earth-directed coronal mass ejections at in situ spacecraft using COR and HI observations from STEREO. *The Astrophysical Journal*, *772*, 70. https://doi.org/10.1088/0004-637X/772/1/70

Miyake, W., Saito, T., Hayakawa, H., & Matsuoka, A. (2005). On the correlation of the solar wind observed at the L5 point and at the Earth. *Advances in Space Research*, *12*, 2328–2332.

Oughton, E., Copic, J., Skelton, A., Kesaite, V., Yeo, Z. Y., Ruffle, S. J., et al. (2016). *Helios Solar Storm scenario*: Cambridge Risk Framework series, Centre for Risk Studies. Cambridge, UK: University of Cambridge.

Owens, M. J., Challen, R., Methven, J., Henley, E., & Jackson, D. R. (2013). A 27 day persistence model of near-Earth solar wind conditions: A long lead-time forecast and a benchmark for dynamical models. *Space Weather*, *11*, 225–236. https://doi.org/10.1002/swe.20040

Richardson, I. G., & Cane, H. V. (2010). Near-Earth interplanetary coronal mass ejections during solar cycle 23 (1996 - 2009): Catalog and summary of properties. *Solar Physics*, *264*, 189–237.

Roebber, P. J. (1998). The regime dependence of degree dat forecast technique, skill, and value. *Weather and Forecast*, *13*, 783–794.

Savani, N. P., Davies, J. A., Davis, C. J., Shiota, D., Rouillard, A. P., Owens, M. J., et al. (2012). Observational tracking of the 2D structure of coronal mass ejections between the Sun and 1 AU. *Solar Physics*, *279*, 517–535.

Scrijver, C. J., & De Rosa, M. L. (2003). Photospheric and heliospheric magnetic fields. *Solar Physics*, *212*, 165–200.

Simunac, K. D. C., Kistler, L. M., Galvin, A. B., Popecki, M. A., & Farrugia, C. J. (2009). In-situ observations from STEREO/PLASTIC: A test for L5 space weather monitors. *Annals of Geophysics*, *27*, 3805–3809.

Thomas, S. R., Owens, M. J., & Lockwood, M. (2014). The 22-year Hale cycle in cosmic ray flux—Evidence for direct heliospheric modulation. *Solar Physics*, *289*, 407–421. https://doi.org/10.1007/s11207-013-0341-5

Thomas, S. R., Owens, M. J., Lockwood, M., Barnard, L., & Scott, C. J. (2015). Near-Earth cosmic ray decreases associated with remote coronal mass ejections. *The Astrophysical Journal*, *801*, 5. https://doi.org/10.1088/0004-637X/801/1/5

Trichas, M., Gibbs, M., Harrison, R., Green, L., Eastwood, J., Bentley, B., et al. (2015). Carrington-L5: The UK/US operational space weather monitoring mission. *Hipparchos*, *2*(12), 25–31.

Tsurutani, B. T., Gonzalez, W. D., Gonzalez, A. L. C., Guarnieri, F. L., Gopalswamy, N., Grande, M., et al. (2006). Corotating solar wind streams and recurrent geomagnetic activity: A review. *Journal of Geophysical Research*, *111*, A07S01. https://doi.org/10.1029/2005JA011273

Tucker-Hood, K., Scott, C. J., Owens, M. J., Jackson, D., Barnard, L., Davies, J. A., et al. (2015). Validation of a priori CME arrival predictions made using real-time heliospheric imager observations. *Space Weather*, *13*, 35–48. https://doi.org/10.1002/2014SW001106

Turner, D. L., & Li, X. (2011). Using spacecraft measurements ahead of Earth in the Parker spiral to improve terrestrial space weather forecasts. *Space Weather*, *9*, S01002. https://doi.org/10.1029/2010SW000627

Webb, D. F., & Howard, T. A. (2012). Coronal mass ejections: Observations. *Living Reviews in Solar Physics*, *9*, 3. http://www.livingreviews.org/lrsp-2012-3

Wicks, R. T., Roberts, D. A., Mallet, A., Schekichihin, A. A., Horbury, T. S., & Chen, C. H. K. (2013). Correlations at large scales and the onset of turbulence in the fast solar wind. *The Astrophysical Journal*, *778*, 177. https://doi.org/10.1088/0004-637X/778/2/177

Zhang, X. Y., Moldwin, M. B., Steinberg, J. T., & Skoug, R. M. (2014). Alfvén waves as a possible source of long-duration, large-amplitude, and geoeffective southward IMF. *Journal of Geophysical Research: Space Physics*, *119*, 3259–3266. https://doi.org/10.1002/2013JA019623

Zou, Y., Donner, R. V., Marwan, N., Small, M., & Kurths, J. (2014). Long-term changes in the north-south asymmetry of solar activity: A nonlinear dynamics characterization using visibility graphs. *Nonlinear Processes in Geophysics*, *21*, 1113–1126.